Cluster Abundance Constraints on Quintessence Models

Limin Wang and Paul J. Steinhardt

Department of Physics and Astronomy, University of Pennsylvania, Philadelphia, Pennsylvania 19104 USA

ABSTRACT

The abundance of rich clusters is a strong constraint on the mass power spectrum. The current constraint can be expressed in the form $\sigma_8 \Omega_m^\gamma = 0.5 \pm 0.1$ where σ_8 is the rms mass fluctuation on 8 h^{-1} Mpc scales, Ω_m is the ratio of matter density to the critical density, and γ is model-dependent. In this paper, we determine a general expression for γ that applies to any models with a mixture of cold dark matter plus cosmological constant or quintessence (a time-evolving, spatially-inhomogeneous component with negative pressure) including dependence on the spectral index n, the Hubble constant h, and the equation-of-state of the quintessence component w. The cluster constraint is combined with COBE measurements to identify a spectrum of best-fitting models. The constraint from the evolution of rich clusters is also discussed.

Subject headings: cosmology: theory - dark matter - large-scale structure of universe - galaxies: clusters: general - X-rays: galaxies

1. Introduction:

Rich clusters can be used to constrain cosmological models of large-scale structure formation. Rich clusters are the largest virialized objects in the universe and, hence, their abundance and evolution can be simply related to the linear mass power spectrum, $P(k)$. Their x-ray temperature can be used to infer the cluster mass. Then, Press-Schechter (1974) theory can be used to relate the observed cluster abundance as a function of mass to the rms fluctuation on $8\ h^{-1}$ Mpc scales, σ_8. The result is a constraint on a combination of parameters, $\sigma_8 \Omega_m^\gamma$, where γ is a function of model parameters.

In this paper, we obtain a general expression for γ which applies to a wide range of models including the standard cold dark matter (sCDM) model, models with a mixture of cosmological constant (Λ) and cold dark matter (ΛCDM), and QCDM models with a mixture of cold dark matter and quintessence, a dynamical, time-evolving, spatially inhomogeneous component with negative pressure. An example of quintessence would be a scalar field (Q) rolling down a potential $V(Q)$. It has been shown that a spectrum of ΛCDM and QCDM models satisfy all current observational constraints (Wang et al. 1998). Our expression for γ includes dependence on the spectral index n, the Hubble constant h (in units of 100 km sec^{-1} Mpc^{-1}), and the equation-of-state of the quintessence component w.

In Section 2, we discuss our derivation of the cluster abundance constraint, which follows earlier derivations to some degree but includes some new features when applied to quintessence. Some may wish to proceed directly to the resulting constraint, given in Section 3. Our result appears to differ slightly from some earlier works, but we explain in this section the reasons for those differences. Our purpose in determining γ is to transform observations into a powerful constraint on models. In Section 4, we discuss the further constraint derived from studying the evolution of cluster abundance from redshift $z = 0$ to $z \sim 1$. In Section 5, we conclude by applying the cluster abundance constraint on σ_8 in combination with the constraint on COBE normalization of $P(k)$ to pick out a spectrum of best-fitting ΛCDM and QCDM models.

2. Derivation of the Cluster Abundance Constraint for Quintessence Models

In this section, we present the derivation of the cluster abundance constraint on σ_8 for QCDM models. We take a pedagogical approach in which we first discuss each step for a ΛCDM model and then point out the differences that arise in QCDM models. The final result can be found in Section 3.

2.1. Mass-temperature relation

Press-Schechter theory relates the number density of clusters to their mass. Observations determine directly the temperature instead of the mass of clusters. Therefore, the mass-temperature relation derived from the virial theorem (Lahav et al. 1991; Lilje 1992) is used to apply the Press-Schechter relation.

First, let's consider a universe with vacuum energy density ρ_Λ. For a spherical overdensity, we have

$$T_{vir} = -\frac{1}{2}U_G + U_\Lambda \tag{1}$$

where T_{vir} is the kinetic energy, U_G is the potential energy associated with the spherical mass overdensity, and U_Λ is the potential energy associated with Λ. The kinetic energy is $T_{vir} = \frac{1}{2}M\bar{V}_{vir}^2$ where M is the mass of the cluster and $\bar{V}_{vir}^2$ is the mean square velocity of particles in the cluster. The gravitational potential is $U_G = -\frac{3}{5}\frac{GM^2}{R}$ where G is the gravitational constant and R is the radius of the cluster. The potential due to vacuum energy is $U_\Lambda = -\frac{4}{5}\pi G\rho_\Lambda MR^2$. Re-expressing the background matter energy density at redshift z as $\rho_b = \frac{3H_0^2}{8\pi G}\Omega_0(1+z)^3$ where H_0 the is the Hubble parameter, Ω_0 is the ratio of the matter density to the critical density, and z is the redshift, the virial relation (1) becomes:

$$\bar{V}_{vir}^2 = \frac{3}{5}\left(GMH_0\sqrt{\Omega_0\Delta_c/2}\right)^{2/3}(1+z)\left(1 - \frac{2}{\Delta_c}\frac{\Omega_\Lambda(z)}{\Omega_m(z)}\right) \tag{2}$$

where $\Delta_c \equiv \rho_{cluster}/\rho_b$ is the ratio of the cluster to background density, and $\Omega_\Lambda(z)$ and $\Omega_m(z)$ are the density parameters for vacuum energy and matter at redshift z, respectively. The observed temperature of the gas is

$$k_BT = \frac{\mu m_p}{\beta}\sigma_{los}^2 = \frac{\mu m_p}{\beta}\frac{\bar{V}_{vir}^2}{3} \tag{3}$$

where μm_p is the mean mass of particles; σ_{los}^2 is the line-of-sight velocity dispersion; β is the ratio of the kinetic energy to the temperature and k_B is the Boltzmann constant. The mass of the cluster is then:

$$M = \left(\frac{k_BT}{0.944 f_\beta\,\mathrm{keV}}\right)^{3/2}\left[(1+z)^3\Omega_0\Delta_c\right]^{-1/2}\left[1 - \frac{2}{\Delta_c}\frac{\Omega_\Lambda(z)}{\Omega_m(z)}\right]^{-3/2}h^{-1}10^{15}M_\odot \tag{4}$$

where $f_\beta \equiv f_u\mu/\beta$ where f_u is a fudge factor of order unity that allows deviation from the simplistic spherical model. Using this relation, the mass-temperature relation of a virialized cluster can be computed at any z. However, if we evaluate at redshift $z = z_c$, twice the turn-around time (that is, $t(z_c) = 2t(z_{ta})$ where z_{ta} is the redshift at which the cluster turns around, $\dot{R} = 0$), then $\Delta_c(z_c, \Omega_m) = \Delta_c(\Omega_m)$ becomes a function of Ω_m only (for Λ and open

universes). Note that z_c is the redshift at which the cluster formally collapses to $R = 0$ according to an unperturbed spherical solution.

In quintessence models, the principal difference is that the energy density in Q decreases with time, whereas vacuum energy remains constant. The Q-component does not cluster on scales less than 100 Mpc (Caldwell, Dave, & Steinhardt 1998). Consequently, the only effect of Q on the abundance of rich clusters with size less than 100 Mpc is through its modification of the background evolution. We will restrict ourselves to cases where the equation-of-state w is constant or slowly varying. In this case, the ratio $\Omega_\Lambda(z)/\Omega_m(z)$ above can be replaced by $(1 + z)^{3w}\Omega_Q(z = 0)/\Omega_0$.

For quintessence models, the ratio of cluster to background density, $\Delta_c|_{z_c} = \Delta_c(\Omega_m, w)$, is a function of two variables:

$$\Delta_c(z = z_c) \equiv \frac{\rho_{cluster}(z_c)}{\rho_b(z_c)} = \zeta \left(\frac{R_{ta}}{R_{vir}}\right)^3 \left(\frac{1 + z_{ta}}{1 + z_c}\right)^3. \tag{5}$$

where $\zeta \equiv \rho_{cluster}(z_{ta})/\rho_b(z_{ta})$; R_{ta} and R_{vir} are the radius of the cluster at $z = z_{ta}$ and at virialization, respectively. (The second equality utilizes the standard assumption that the cluster has virialized at $z = z_c$.) The factor ζ has been computed by solving for the evolution of a spherical overdensity in a cosmological model with constant w (see Appendix A). We find that ζ is weakly model-dependent: $\zeta = (3\pi/4)^2\Omega_m^{-0.79+0.26\Omega_m-0.06w}|_{z_{ta}}$ for $-1 \leq w \leq 0$. The fact that this expression is weakly model-dependent means that we can also apply it to models with time-varying w.

By the virial theorem and energy conservation, we have:

$$\frac{1}{2}U_G(z_c) + 2U_Q(z_c) = U_G(z_{ta}) + U_Q(z_{ta}) \tag{6}$$

This leads to an approximate solution

$$\frac{R_{vir}}{R_{ta}} = \frac{1 - \eta_v/2}{2 + \eta_t - 3\eta_v/2} \tag{7}$$

where $\eta_t = 2\zeta^{-1}\Omega_Q(z_{ta})/\Omega_m(z_{ta})$ and $\eta_v = 2\zeta^{-1}((1 + z_c)/(1 + z_{ta}))^3\Omega_Q(z_c)/\Omega_m(z_c)$. The fact that η_v is time-dependent if $w \neq -1$ is because the energy within the cluster is not exactly conserved and the temperature is shifting after virialization due to the change in the Q-energy, ρ_Q, within the cluster. However, since the matter density ρ_m is much larger than ρ_Q in a collapsed cluster, this correction is negligible.

2.2. Density Dispersion

The dispersion of the density field on a given comoving scale R is

$$\sigma^2(R, z) = \int_0^\infty W^2(kR)\Delta^2(k, z)\frac{d\,k}{k} \tag{8}$$

where

$$W(kR) = 3\left(\frac{sin(kR)}{(kR)^3} - \frac{cos(kR)}{(kR)^2}\right)r, . \tag{9}$$

and

$$\Delta^2(k, z) = 4\pi k^3 P_\delta(k, z). \tag{10}$$

$P_\delta(k) \equiv |\delta_k|^2$ is the power spectrum and δ_k is the Fourier transform of the fractional density perturbation $(\delta\rho/\rho)^2 \equiv \langle\delta^2(\vec{x})\rangle$

$$\delta_k \equiv \delta(|\vec{k}|) = \frac{1}{(2\pi)^{3/2}}\int d^3x \delta(\vec{x})e^{i\vec{k}\cdot\vec{x}}. \tag{11}$$

For constant or slowly varying $w < -1/3$, the BBKS approximation to the power spectrum (Bardeen et al. 1986) is reliable. However, if $w > -1/3$ or if w is rapidly varying, we find no general fitting formula; instead, $P(k)$ must be obtained numerically.

The *rms* mass fluctuation $\sigma_8(z) \equiv \sigma(R = 8h^{-1}Mpc, z)$ can be expressed as $\sigma_8(z) = g(z)\sigma_8(z = 0)$, where $g(z)$ is the growth factor. The growth factor is proportional to the linear density perturbation $\delta_\rho \equiv \delta\rho/\rho$ and normalized to $g(z = 0) = 1$. We find that a good approximation to the the growth index is given by (see Appendix B)

$$f_g \equiv \frac{d\,\ln\delta_\rho}{d\,\ln a} = \Omega_m(z)^\alpha \tag{12}$$

where $a = 1/(1 + z)$ is the scale factor and

$$\alpha = \frac{3}{5 - \frac{w}{1-w}} + \frac{3}{125}\frac{(1 - w)(1 - 3w/2)}{(1 - 6w/5)^3}(1 - \Omega_m) + \mathcal{O}((1 - \Omega_m)^2) \tag{13}$$

The growth factor $g(z)$ is obtained from the integral expression

$$g(z) \approx a\,\exp\left[\int_a^1 \frac{da}{a}(1 - \Omega_m^\alpha)\right] \tag{14}$$

We tested the expression for g obtained from Eq. (13) against the value obtained by numerically integrating the density perturbation equations; for $1 - \Omega_m$ between zero and 0.8, the accuracy is better than 1%.

2.3. Press-Schechter Theory

According to Press-Shechter theory, the comoving number density of virialized objects with mass $M = 4\pi R^3 \rho_b/3$ is:

$$d\,n(M,z) = -\sqrt{\frac{2}{\pi}}\frac{\rho_b}{M^2}\frac{\delta_c R}{3\sigma^2(R,z)}\frac{d\,\sigma(R,z)}{d\,R}\exp\left[-\frac{\delta_c^2}{2\sigma^2(R,z)}\right]d\,M \qquad (15)$$

where $\delta_c = \rho_{linear}/\rho_b$ is the perturbaton that would be predicted for a spherical overdensity of radius R and mass M according to linear theory. Given the observed number density Δn within a certain temperature range ΔT, Eqs. (4) and (15) can be used to determine the normalization of the mass power spectrum σ_8.

The major uncertainties in this method are the observational error in the number density Δn and the systematic error in determining the model parameters δ_c in Eq. (15) and f_β in Eq. (4). Specifically

$$\frac{\delta\sigma_8}{\sigma_8} = u_1\frac{\delta\Delta n}{\Delta n} + \frac{\delta(\delta_c)}{\delta_c} - \left[\left(1 + \frac{u_2 + u_3}{2}\right)u_1 - \frac{u_2}{2}\right]\frac{\delta f_\beta}{f_\beta} \qquad (16)$$

where $u_1 = [\delta_c^2/\sigma(R)^2 - 1]^{-1}$, $u_2 = -d\ln\sigma(R)/d\ln R$ and $u_3 = -d\ln\sigma(R)'/d\ln R$ are positive and of order unity in the range of interest. By studying spherical models, we find that δ_c varies slowly as a function of Ω_m, $1.6 < \delta_c < 1.686$. We also find that f_β does not depend on the cosmological model and can be determined by numerical simulation.

According to Eq. (4), the virial temperature corresponding to a given virial mass depends on the redshift at which a cluster is virialized. Therefore, to get the number density of clusters of a given temperature range today, we need to find out the virialization rate and integrate from $z = 0$ to $z = \infty$. Assuming that the merger of clusters is negligible, the Press-Schechter relation, Eq. (15) can be re-expressed as:

$$\frac{d\,n(T,z)}{dz} = -\sqrt{\frac{1}{2\pi}}\frac{\rho_b}{M(T,z)T}\frac{d\,\ln\sigma(R,z)}{d\ln R}\frac{d\,\ln\sigma_8(z)}{dz}x(x^2-1)e^{-\frac{x^2}{2}}d\,T \qquad (17)$$

where $x = \delta_c/\sigma(R,z)$.

Lacey & Cole (1993,1994) and Sasaki (1994) have estimated the corrections due to cluster merging (see also, Viana & Liddle 1996). The corrections are small. In our results, we average the two estimates of the merging correction to obtain our final result.

3. Generalized Cluster Abundance Constraint

The cluster abundance constraint on σ_8 is obtained by comparing the theoretical prediction discussed in the previous section to observations. The observed X-ray cluster abundance as a function of temperature was presented by Edge et al (1990) and Henry & Arnaud (1991, hereafter HA). After a recent correction (Henry 1997) to HA, the two results agree. We have fit the theoretically predicted number density *vs.* temperature curve (the temperature function) to the HA data.

3.1. Principal Results

Our results can be fit by

$$\sigma_8 = (0.50 - 0.1\Theta)\Omega^{-\gamma(\Omega,\Theta)} \tag{18}$$

where $\Theta \equiv \Theta_n + \Theta_h = (n_s - 1) + (h - 0.65)$ where n_s is the spectral index of primordial energy density perturbations and h is the present Hubble constant in units of $100\,\mathrm{km\,s^{-1}\,Mpc^{-1}}$. For QCDM models with equation-of-state w (including ΛCDM with $w = -1$), our fit to γ is

$$\gamma(\Omega, \Theta) = 0.21 - 0.22w + 0.33\Omega + 0.25\Theta. \tag{19}$$

For open models

$$\gamma(\Omega, \Theta) = 0.33 + 0.35\Omega + 0.20\Theta. \tag{20}$$

3.2. Comparison to Previous Computations

Many groups have presented similar constraints on σ_8 for ΛCDM and OCDM models. In general, all of them are in reasonable agreement with one another and with our result. We identify below the sources of the discrepancies, some real and some only apparent, when compared to White, Efstatiou, & Frenk (1993, hereafter WEF); Eke, Cole, & Frenk (1996, hereafter ECF); Viana and Liddle (1996, hereafter VL); Pen (1997, hereafter Pen); Kitayama and Suto (1997, hereafter KS).

(1) As we argued, an integration (with merger correction) of Eq. (17) is necessary since the mass-temperature relation is redshift dependent. Most groups only applied Eqs. (4) and (15) at redshift $z = 0$ to obtain their main results, which leads to an overestimate of σ_8 by as much as 10%. However, some groups (ECF and Pen) fit the number density and temperature relations to numerical simulations to normalize their coefficient f_β in Eq. (4).

In so doing, they effectively incorporated the integration correction into the coefficient f_β for the cases that were numerically tested. Consequently, their fitted value of f_β does not represent precisely $f_u \mu / \beta$ as defined in Eq. (4). We shall call their corresponding coefficient $\tilde{f}_\beta$ to emphasize that the physical meaning of this coefficient has been modified to include intregration over redshift. Since the contribution of the integration is not proportional to f_β in all cosmological models, it is more precise and physically meaningful to do separately the redshift integration.

(2) The shape of the theoretical cluster temperature function, Eq. (17), does not agree equally well with observations for all parameters. The fit is particularly poor for models with large $\Gamma \equiv \Omega_m h$ and positive tilt ($n_s > 1$). To handle this problem, some groups (WEF; Pen; VL) only fit the observed number density at one particular temperature; this introduces some arbitrariness and leads to much larger uncertainties depending on which temperature is chosen. In our analysis, we fit the theoretical temperature function to all the data points provided by HA.

(3) The recent correction to the HA data results in a correction to the VL results of 20%.

(4) Most groups (WEF; ECF; VL; Pen) assume a fixed "shape parameter" $\Gamma = \Omega_m h$. We found that no single Γ is valid for all QCDM models. Instead of expressing our results in terms of fixed Γ, we fix $h = 0.65$. We include the dependence on h (Θ_h) explicitly.

(5) Most recent analyses (ECF; VL; Pen; KS) adopted similar modeling of the mass-temperature relation. However, there is still about 10% to 20% disagreement on the value of f_β in Eq. (4) due to the uncertainties of the numerical simulations. We found that the most extensive simulation results, those of ECF and Pen, agree very well with each other. By normalizing our theoretical calculations to their simulations, we found $f_\beta = 1.1$. Notice that their reported values for the coefficient are $\tilde{f}_\beta = 1.4$ and $\tilde{f}_\beta = 1.3$, respectively. This discrepancy is due to rolling into $\tilde{f}_\beta$ the integration effect described under (1). Recent simulations by Bryan and Norman (1997) also indicate a similar result, once one corrects for their slightly higher value of δ_c.

(5) Some groups (VL) used the differential temperature function (the cluster abundance within unit temperature interval around a center value T_{cen}) while others (WEF; ECF; Penn; KS) used cumulative temperature function (the cluster abundance with temperature above a critical temperature T_{cri}). These two approaches give similar results because the cluster abundance drops exponentially with temperature and the cumulative cluster abundance is well approximated by counting the cluster abundance around T_{cri}. We compared the results obtained by using the differential temperature function given by HA and that obtained by using the cumulative temperature function provided by ECF and

found them to be in good agreement. However, the error bar of the latter is much smaller: most models were excluded by 95% confidence level by the temperature function fitting. To be conservative, we used the former to get our results and errors.

3.3. Error Estimates

Eq. (16) can be used to estimate the total error for σ_8. From the present scatter of numerical simulation results, f_β has about 20% uncertainty, δ_c has about 10% uncertainty and another 15% uncertainty comes from the observation. Therefore, the net uncertainty quoted in Eq. (18) is about 20% corresponding to 95% confidence level.

4. Evolution of Abundance

By applying the same theoretical tools, we can also study the evolution of the cluster abundance to obtain further constraints on σ_8 and Ω_m. The current redshift survey results were converted to number densities of clusters with their comoving-1.5 mass (the mass within comoving radius $R_{com} = 1.5h^{-1}Mpc$) greater than a given mass threshold $M_{1.5}$ (Carlberg et al. 1997; Bahcall, Fan, & Cen 1997). If the mass profile for the cluster obeys $M(R) \propto R^p$ near $R = 1.5h^{-1}Mpc$, and the average virial overdensity is equal to Δ_c as calculated in Eq. (5), then the virial mass M is related to $M_{1.5}$ by

$$M = \left(\frac{178}{\Delta_c} \frac{M_{1.5}}{6.97 \times 10^{14}\Omega_0 h^{-1}M_\odot} \right)^{\frac{p}{3-p}} M_{1.5} \tag{21}$$

Eq. (15) can be used to estimate the number density of observed objects at a given redshift. We adopted $p = 0.64$ as suggested by Carlberg, Yee, & Ellingson (1997).

The log-abundance as a function of z, $\log_{10}\left(n(M_{1.5}, z)\right)$, is roughly linear as a function of z for $0 < z < 1$ for the models of interest. A useful parameter to characterize the evolution of cluster abundance at redshift $0 \leq z \leq 1$ is $A(M_{1.5})$, defined by

$$\log_{10}\left(n(M_{1.5}, z)\right) \approx A(M_{1.5})z + B(M_{1.5}) \tag{22}$$

where $n(M_{1.5}, z)$ is the number density of clusters with comoving-1.5 mass greater than $M_{1.5}$ observed at redshift z. The smaller $A(M_{1.5})$ is, the stronger the evolution is. By applying this analysis to models, we found
(1) Cluster abundance evolution strongly depends on σ_8: low σ_8 leads to strong evolution. This agrees with what Bahcall, Fan, & Cen (1997) have found. This is a general feature of

Gaussian-distributed random density peaks.

(2) Cluster abundance is also sensitive to the equation-of-state of quintessence w: low w leads to strong evolution. With the same Ω_0, the growth of density perturbations gets suppressed earlier in high w models, therefore, they have a weaker evolution in recent epochs ($0 \leq z \leq 1$).

In Figure 1, we show $A(M_{1.5} = 8 \times 10^{14}h^{-1}Mpc)$ as a function of σ_8 for some sample models which have been chosen because they all fit current observations well (see discussion in following section). We allow σ_8 to vary from 0.5 to 1.0 with the COBE normalized σ_8 shown as opaque circles. The current redshift survey data (Bahcall & Fan 1998) indicate $A(M_{1.5} = 8 \times 10^{14}h^{-1}Mpc) \gtrsim -5$ at the 3σ level (with mean equal to -1.7), which is consistent with all six COBE normalized models.

5. Conclusions

The cluster abundance and evolution constraints, when combined with future measurements of the cosmic microwave background, may be an effective means of discriminating quintessence and Λ models.

The cosmic microwave background (CMB) anisotropy provides a constraint on the mass power spectrum on the horizon scale. For a given model, this constraint from large-scale anisotropy as measured by the COBE-DMR satellite (Smoot et al. 1992; Bennett et al. 1996) can be extrapolated to obtain a limit on σ_8 that is completely independent of the cluster abundance constraint. In Figure 2, we plot the dependence of σ_8 on Ω_Q. For each w, a different curve is shown. Along each curve is highlighted the range of $\sigma_8 - \Omega_Q$ consistent with the cluster abundance constraint derived in this paper. Hence, the best-fit models are those near the middle of the highlighted regions. These are the same models used as examples in Figure 1.

Near future satellite experiments, such as the NASA Microwave Anisotropy Probe (MAP) and the ESA Planck mission, will greatly improve upon COBE by determining the temperature anisotropy power spectrum to extremely high precision from large to small angular scales. Even a full-sky, cosmic variance limited measurement of the CMB anisotropy, though, may not be sufficient to discriminate ΛCDM from QCDM models. There is a degeneracy in parameter space such that, for any given ΛCDM models, there is a continuous family of QCDM models which predicts the same CMB power spectrum (Huey et al. 1998; White 1998) It is possible that the data points to a QCDM model, say, which

lies outside this degenerate set of models, *e.g.*, a model with rapidly varying w. However, if the data points to the degenerate set of models, then it is critically important to find a method of discriminating models further. Not only does degeneracy mean that Λ cannot be distinguished from quintessence, but also that large uncertainty in Ω_m and h. Here we wish to illustrate how cluster abundance may play an important role.

An example of a "degeneracy curve" is shown in Figure 3. Given a value of h for any one point along the curve, values of h can be chosen for other points along the curve such that the models are all indistinguishable from CMB measurements. The near-future satellites are capable of limiting parameter space to a single degeneracy curve. The CMB anisotropy also narrowly constrains n_s, $\Omega_b h^2$, and $\Omega_m h^2$. However, even when combined with the cluster abundance constraint and other cosmological constraints from the age, Hubble constant, baryon fraction, Lyman-α opacity, deceleration parameter and mass power spectrum, a substantial degeneracy can remain. Figure 3 includes a shaded region which exemplifies the range which these models might allow, based on current measurements (Wang et al. 1998; Huey et al. 1998). Because of the uncertainty in cluster abundance at $z = 0$ and other cosmic parameters, the overlap between the degeneracy curve and the shaded region allows a wide range of Ω_m, h and w.

Cluster evolution offers a promising approach for breaking the degeneracy. Figure 4 illustrates the variation of $A(M_{1.5})$ as a function of w for models along the degeneracy curve and inside the shaded region of Figure 3. The variation in $A(M_{1.5})$ is nearly 2, corresponding to nearly two orders of magnitude variation in abundance at redshift $z = 0.5$. The range of $A(M_{1.5})$ is between -3.5 and -5.5 in this case, but this could be shifted upward or downward by adjusting cosmic parameters. The point is that models which are degenerate in terms of CMB anisotropy are spread out in $A(M_{1.5})$. If the measurements can be refined so that $A(M_{1.5})$ is know to better than ± 0.5, then cluster evolution may play an important role in discriminating between quintessence and vacuum density and, thereby, determining Ω_m and h.

REFERENCES

Bahcall, N.A., Fan, X., & Cen, R. 1997,ApJ,485,L53

Bahcall, N.A., & Fan, X. 1998,ApJ,in press,astro-ph/9803277

Bardeen, J.M., Bond, J.R., Kaiser, N., & Szalay, A.S. 1986,ApJ,304,15

Bennett, C.L. et al. 1996,ApJ,464,L1

Bryan, G.L., & Norman, M.L. 1997,astro-ph/9710107

Caldwell, R.R., Dave, R., & Steinhardt, P.J. 1998,in preparation

Carlberg, R.G., Morris, S.M., Yee, H.K.C., & Ellingson, E. 1997,ApJ,479,L19

Carlberg, R.G., Yee, H.K.C., & Ellingson, E. 1997,ApJ,478,462

Edge, A.C., Stewart, G.C., Fabian, A.C., & Arnaud, K.A. 1990,MNRAS,245,559

Eke, V.R., Cole, S., & Frenk, C.S. 1996,MNRAS,282,263

Henry, J.P. 1997,ApJ,489,L1

Henry, J.P., & Arnaud, K.A. 1991,ApJ,372,410

Huey, G., Wang, L., Dave, R., Caldwell, R.R., & Steinhardt, P.J. 1998,in preparation

Kitayama, T., & Suto, Y. 1997,ApJ,490,557

Lacey, C., & Cole, S. 1993,MNRAS,262,627

Lacey, C., & Cole, S. 1994,MNRAS,271,676

Lahav, O., Lilje, P.B., Primack, J.R., & Rees, M.J. 1991,MNRAS,251,128

Lilje, P.B. 1992,ApJ,386,L33

Pen, U.-L. 1997,astro-ph/9610147

Press, W.H., & Schechter, P. 1974,ApJ,187,452

Sasaki, S. 1994,PASJ,46,427

Smoot, G. et al. 1992,ApJ,396,L1

Viana, P.T.P., & Liddle, A.R. 1996,MNRAS,281,323

Wang, L, Caldwell, R.R., Ostriker, J.P., & Steinhardt, P.J. 1998,in preparation

White, M 1998, astro-ph/9802295

White, S.D.M., Efstathiou, G., & Frenk, C.S. 1993,MNRAS,262,1023

A.   Spherical Model

We study a spherical overdensity with uniform matter density $\rho_{cluster}$ and radius R in a background that satisfies the Friedmann equation:

$$\left(\frac{\dot{a}}{a}\right)^2 = \frac{8\pi G}{3}(\rho_b + \rho_Q) \tag{A1}$$

where a is the scale factor, ρ_b is the background matter energy density and ρ_Q is the energy density in Q. Quintessence doesn't cluster at the interesting scales; the energy density in Q remains the same both inside and outside the overdensity patch. Because the curvature is not a constant inside the overdensity patch. we use the time-time component of the Einstein equations (which does not involve the curvature term) to solve for the growth of the overdensity patch

$$
\begin{aligned}
\frac{\ddot{R}}{R} &= -4\pi G\left(p_Q + \frac{\rho_Q + \rho_{cluster}}{3}\right) \\
&= -4\pi G\left[\left(w + \frac{1}{3}\right)\rho_Q + \frac{1}{3}\rho_{cluster}\right]
\end{aligned}
\tag{A2}
$$

We have used $p_Q = w\rho_Q$ to obtain the second equality. Now, we define

$$x \equiv \frac{a}{a_{ta}} \tag{A3}$$

$$y \equiv \frac{R}{R_{ta}} \tag{A4}$$

where a_{ta} and R_{ta} are the scale factor and the radius at turn-around time, then

$$\rho_b = \frac{3H_{ta}^2}{8\pi G}\frac{\Omega_m(x=1)}{x^3} \tag{A5}$$

$$\rho_Q = \frac{1 - \Omega_m(x)}{\Omega_m(x)}\rho_b \tag{A6}$$

$$\rho_{cluster} = \frac{3H_{ta}^2}{8\pi G}\frac{\Omega_m(x=1)}{y^3}\zeta \tag{A7}$$

where $\Omega_m(x)$ is the matter energy density parameter at x, H_{ta} is the Hubble constant at turn-around time and $\zeta \equiv (\rho_{cluster}/\rho_b)|_{x=1}$. Eqs. (A1) and (A2) can be then written as

$$\frac{d\,x}{d\,\tau} = (a\Omega_m(x))^{-1/2} \tag{A8}$$

$$\frac{d^2 y}{d\tau^2} = -\frac{1}{2}\left[\frac{\zeta}{y^2} + (1+3w)\frac{1 - \Omega_m(x)}{\Omega_m(x)}\frac{y}{x^3}\right] \tag{A9}$$

where $d\tau = H_{ta}\sqrt{\Omega_m(x=1)}dt$. With the boundary condition $dy/d\tau|_{x=1} = 0$ and $y|_{x=0} = 0$, ζ is uniquely determined by Eqs. (A8) and (A9), given the function form of $\Omega_m(x)$. For constant w, we have

$$\Omega_m(x) = \left(1 + \frac{1 - \Omega_m(x=1)}{\Omega_m(x=1)}x^{-3w}\right)^{-1} \tag{A10}$$

and ζ obtained from Eqs. (A8) and (A9) can be well fitted by

$$\zeta = \left(\frac{3\pi}{4}\right)^2 \Omega_m^{-0.79+0.26\Omega_m-0.06w}|_{x=1} \tag{A11}$$

The linear overdensity δ_c at $t(z_c) = 2t(z_{ta})$ can also be calculated by evolving Eqs. (A8) and (A9). At early time, the perturbation is linear

$$\frac{\rho_{cluster}}{\rho_b} = \left(\frac{x}{y}\right)^3 \zeta \xrightarrow{x \to 0} \delta_c(x) \tag{A12}$$

Once δ_c is known at some x_0, then it is easily obtained at an arbitrary time

$$\delta_c(x) = \frac{g(x)}{g(x_0)}\delta_c(x_0) \tag{A13}$$

where g is the growth factor that can be calculated by using Eq. (14).

B. Growth Index in a Quintessense Universe

The Q-component does not participate directly in cluster formation, but it alters the background cosmic evolution. The linear perturbation equation can be written as:

$$\ddot{\delta} + 2\frac{\dot{a}}{a}\dot{\delta} = 4\pi G\rho\delta \tag{B1}$$

where a is the scale factor of the Universe, dot means derivative with respect to physical time t, $\delta = \delta\rho_m/\rho_m$, ρ_m and $\delta\rho_m$ are the density and overdensity of the matter respectively. The background evolution equations in a flat universe are:

$$\left(\frac{\dot{a}}{a}\right)^2 = \frac{8\pi G}{3}(\rho_m + \rho_Q) \tag{B2}$$

$$2\frac{\ddot{a}}{a} + \left(\frac{\dot{a}}{a}\right)^2 = -8\pi Gw\rho_Q \tag{B3}$$

where ρ_Q is the energy density of the Q-component and $w \equiv p_Q/\rho_Q$ is the equation-of-state of the Q-component. Now, we can define a matter energy density parameter $\Omega \equiv \Omega(a)$ so that:

$$H^2 = \left(\frac{\dot{a}}{a}\right)^2 = \frac{8\pi G}{3}\frac{\rho_m}{\Omega} \tag{B4}$$

From Eqs. (B2), (B3) and (B4), we can get:

$$\frac{\ddot{a}a}{\dot{a}^2} = -\frac{1}{2} - \frac{3}{2}w(1 - \Omega) \tag{B5}$$

By using Eqs. (B2), (B4) and conservation of stress energy $d(\rho a^3) = -pd(a^3)$:

$$\frac{d\,\Omega}{d\ln a} = 3w(1 - \Omega)\Omega \tag{B6}$$

By using Eqs. (B1), (B4) and (B5) we get:

$$\frac{d^2 \ln \delta}{d\ln a^2} + \left(\frac{d\ln\delta}{d\ln a}\right)^2 + \frac{d\ln\delta}{d\ln a}\left[\frac{1}{2} - \frac{3}{2}w(1 - \Omega)\right] = \frac{3}{2}\Omega \tag{B7}$$

The growth index f is defined as:

$$f \equiv \frac{d\ln\delta}{d\ln a} \tag{B8}$$

By using Eqs. (B6) and (B7), we are able to get the equation for f in terms of Ω:

$$3w\Omega(1 - \Omega)\frac{d\,f}{d\,\Omega} + f\left[\frac{1}{2} - \frac{3}{2}w(1 - \Omega)\right] + f^2 = \frac{3}{2}\Omega \tag{B9}$$

Now, we introduce variable α, so that $f \equiv \Omega^\alpha$, and Eq. (B9) becomes:

$$3w(1 - \Omega)\Omega\ln\Omega\frac{d\,\alpha}{d\,\Omega} - 3w(\alpha - \frac{1}{2})\Omega + \Omega^\alpha - \frac{3}{2}\Omega^{1-\alpha} + 3w\alpha - \frac{3}{2}w + \frac{1}{2} = 0 \tag{B10}$$

For slowly varying equation-of-state ($|d\,w/d\,\Omega| \ll 1/(1 - \Omega)$), we shall get:

$$\alpha = \frac{3}{5 - \frac{w}{1-w}} + \frac{3}{125}\frac{(1 - w)(1 - 3w/2)}{(1 - 6w/5)^3}(1 - \Omega) + \mathcal{O}((1 - \Omega)^2) \tag{B11}$$

By following a similar derivation, we found that Eq. (B11) is valid for an open universe if we set $w = -1/3$. Hence, α is weakly dependent on Ω_m. The result is $\alpha \approx 6/11$ for ΛCDM (w=-1) and $\alpha \approx 4/7$ for OCDM.
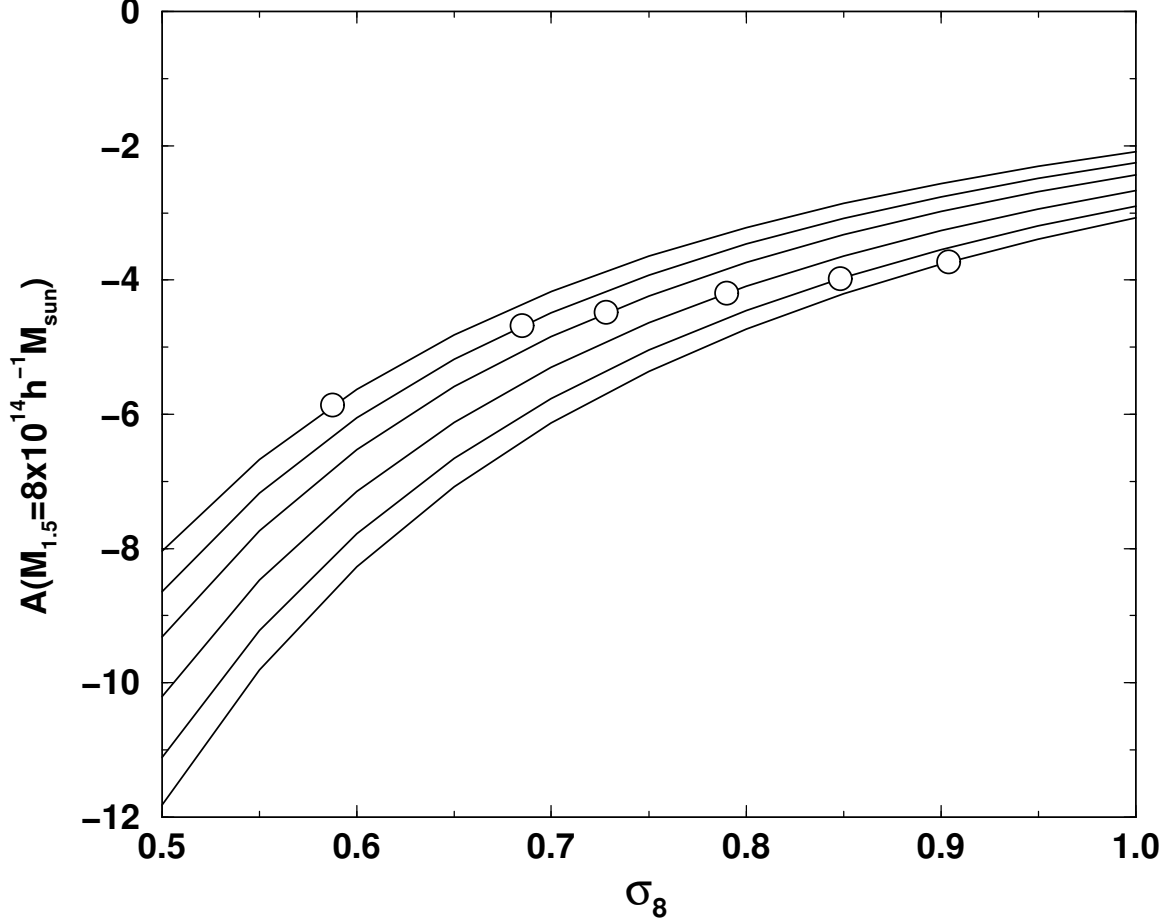
Fig. 1.— The evolution index of cluster abundance for six models selected because they are the best-fit to the combination of COBE and cluster abundance (at $z = 0$) constraints. The model parameters are (from bottom to top): (1) $w = -1$, $\Omega_m = 0.35$, $n_s = 1$, $h = 0.65$, $\Omega_b = 0.047$; (2) $w = -5/6$, $\Omega_m = 0.34$, $n_s = 1$, $h = 0.66$, $\Omega_b = 0.046$; (3) $w = -2/3$, $\Omega_m = 0.35$, $n_s = 1$, $h = 0.66$, $\Omega_b = 0.046$; (4) $w = -1/2$, $\Omega_m = 0.36$, $n_s = 1$, $h = 0.68$, $\Omega_b = 0.043$; (5) $w = -1/3$, $\Omega_m = 0.44$, $n_s = 1$, $h = 0.67$, $\Omega_b = 0.045$; (6) $w = -1/6$, $\Omega_m = 0.49$, $n_s = 1.1$, $h = 0.70$, $\Omega_b = 0.042$.
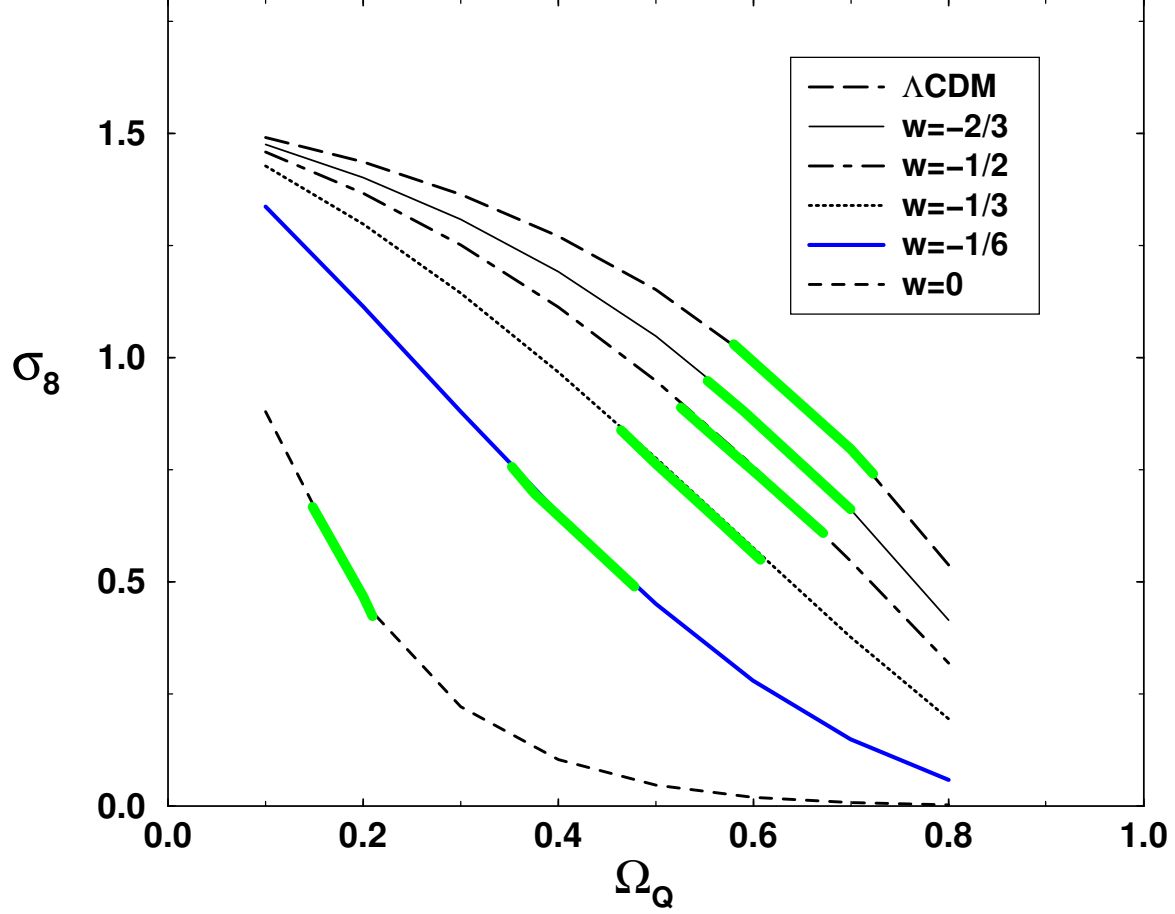
Fig. 2.— COBE-normalized σ_8 as a function of Ω_Q for six constant w models with $n_s = 1$ and $h = 0.65$. They are (from top to bottom): (1) $w = -1$; (2) $w = -2/3$; (3) $w = -1/2$; (4) $w = -1/3$; (5) $w = -1/6$; (6) $w = 0$. The highlighted regions indicate where the x-ray cluster abundance constraints imposed by Eq. (18) overlap the COBE constraint. Best-fit models correspond to the overlap region.
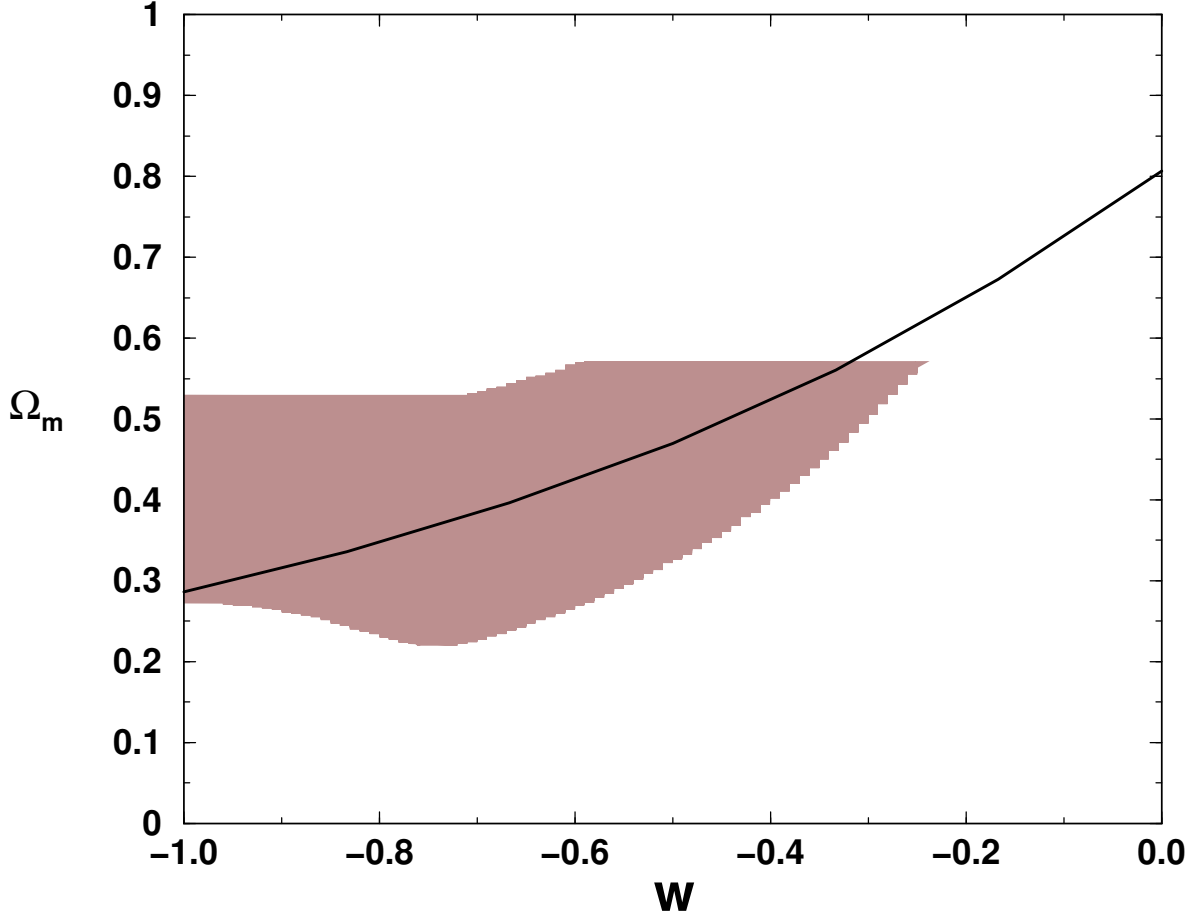
Fig. 3.— Cosmic microwave background (CMB) anisotropy measurements, combined with other constraints on cosmological parameters, may be unable to distinguish among a family of Λ and quintessence models, as illustrated here. All models along the degeneracy curve shown in the figure produce a temperature anisotropy power spectrum that is indistinguishable, given cosmic variance uncertainty. In addition, the CMB can determine other parameters: for this illustration, we have assumed $\Omega_m h^2 = 1.5$, $\Omega_b h^2 = 0.02$ and $n_s = 1$ (reasonable values). Even if these parameters are determined precisely and combined with other observational constraints, there remains substantial uncertainty (shaded region) that may not do much to discriminate among the degenerate models, as illustrated here.
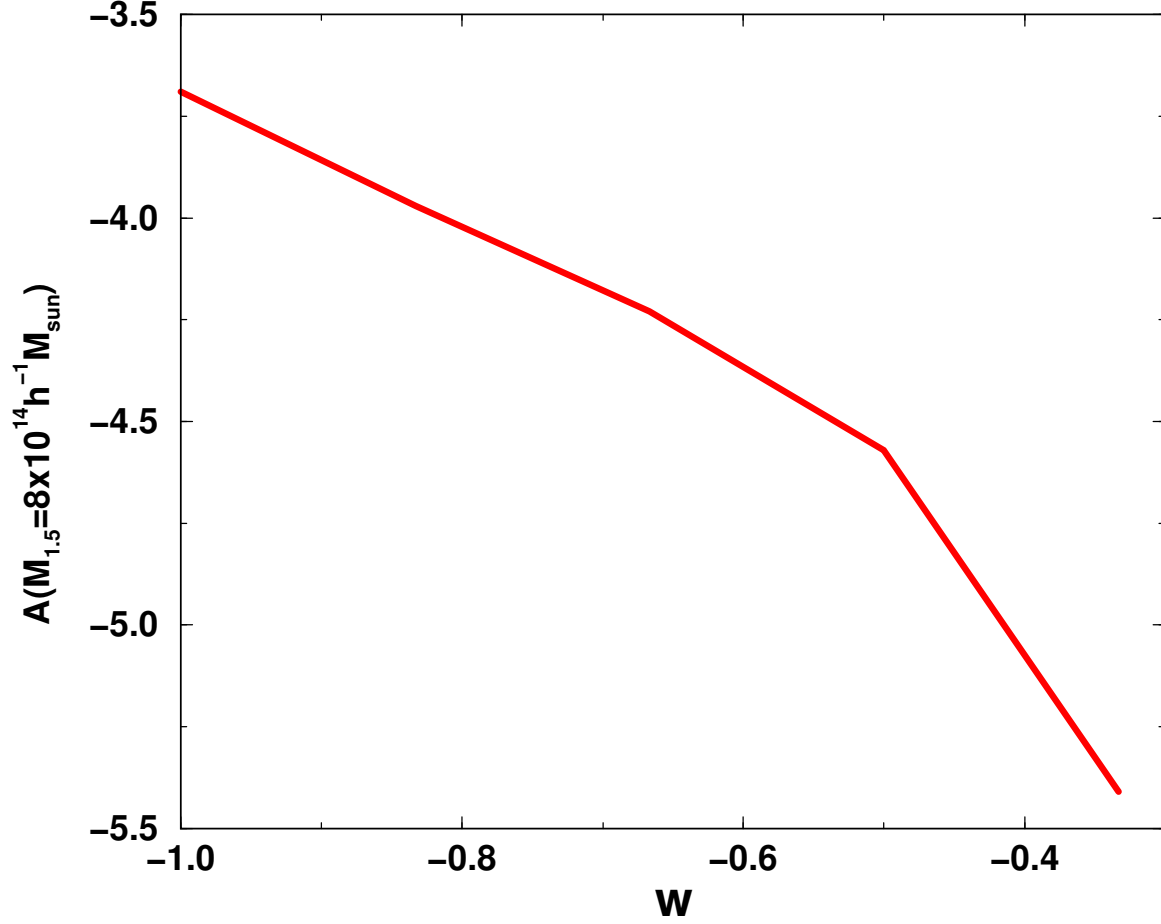
Fig. 4.— The evolution of cluster abundance may break down the degeneracy between Λ and quintessence models illustrated in Fig. 3. $A(M_{1.5})$, the slope of log-abundance *vs.* redshift z, for the models along the degeneracy curve shown in Figure 3.